applied sciences

MDPI

Article

Study of Deformation and Fault Mechanisms in Bedding-Locked Rock Slope

Xiaodong Han, Jinyu Dong *, Xinglong Yang and Huimin Guo

College of Geosciences and Engineering, North China University of Water Resources and Electric Power, Zhengzhou 450045, China; x201710208131@stu.ncwu.edu.cn (X.H.); z201910208188@stu.ncwu.edu.cn (X.Y.); z202210020281@stu.ncwu.edu.cn (H.G.)

* Correspondence: dongjinyu@ncwu.edu.cn

Abstract: In geotechnical engineering, a bedding slope often leads to geological disasters, particularly in the case of bedding-locked rock slopes. This study focuses on a typical bedding-locked rock slope in western Henan Province, China. The deformation and fault characteristics were examined through the development of laboratory analogue experiments which allowed for the analysis of the physical and mechanical properties of the rock slope when subjected to a load. The deformation and faulting mechanisms of the slope were studied through the application of different strength loads to the slope model, as well as through the combination of its physical properties. The deformation and fault process were then simulated through the application of numerical modeling. The results reveal that the upper part of the slope features a linear slip surface, while the lower part features a circular arc slip surface, resulting in "linear + circular arc" damage geometry and a relatively flat shear surface. Maximum and minimum lateral displacement occur around the top and the foot of the slope, respectively, leaving the intermediate values at the middle. The shear strength is greater at the locking section, with the highest value found at the foot of the slope, followed by the middle and the top. The evolution of slope deformation can be divided into three stages: the loose deformation stage at the slope top and back; the stage of crack development, extension, and interlayer misalignment; and the stage of complete through crack formation and complete instability damage of the slope. Thus, the process of the deformation and damage of a rocky slope under loading conditions can be described as follows: load-induced loosening and deformation at the top and back of the slope, crack development, expansion, and interlayer misalignment, as well as tension crack expansion at the foot of the slope. The latter can expand and intensify interlayer misalignment, leading to the destruction of the locking section and ultimately causing the destabilization of the entire slope.

Keywords: locked rock slope; deformation characteristics; physicomechanical properties; numerical analysis

check for updates

Citation: Han, X.; Dong, J.; Yang, X.; Guo, H. Study of Deformation and Fault Mechanisms in Bedding-Locked Rock Slope. *Appl. Sci.* **2024**, *14*, 1786. https://doi.org/10.3390/app14051786

Academic Editor: Nikolaos Koukouzas

Received: 8 January 2024
Revised: 12 February 2024
Accepted: 20 February 2024
Published: 22 February 2024

Copyright: © 2024 by the authors. Licensee MDPI, Basel, Switzerland. This article is an open access article distributed under the terms and conditions of the Creative Commons Attribution (CC BY) license (https://creativecommons.org/licenses/by/4.0/).

1. Introduction

Slope problems have become one of the three most prevalent major global natural disasters due to population growth and overexploitation of the natural environment [1]. Many countries around the world have experienced devastating landslides in recent decades [2,3]. Several alpine countries in Europe, such as Italy and Austria, have experienced serious landslide disasters. Also, landslides often occur in South America, North America, and Asia. In these areas, stratified rock slopes are one of the most common types of slopes. One example of a tragic landslide event occurred on 29th April 1903, in Alberta, Canada, where a slope instability event of 30 million m^3 buried all nearby villages, resulting in the loss of 70 lives [1,4,5]. On 31st May 1970, a rock slide in Peru, triggered by an earthquake, claimed over 18,000 lives. In 1974, one of the largest landslides ever recorded occurred in Peru's Mantaro Valley, with a volume of 1.6 billion cubic meters, resulting in 450 people either missing or dead [4,6–8].

A bedding rock slope is a dipping surface composed of a rock mass with an inclination close to or consistent with the inclination of the bedrock's bedding [9,10]. Several researchers have extensively studied the fault factors and modes of bedding rock slopes due to their impact on engineering construction and human life. Qin Hui et al. (2023) [11] proposed the use of an unloading stress analyzing method (USAM) to determine the sliding surface, safety factor (Fs), and reinforcement force (Fr) of bedding rock slopes. Zhenlin Chen et al. (2020) [12] found that the inclination angle of weak interlayers is a crucial factor that affects the fault mode of rock slopes. Zhang Jipeng et al. (2021) [13] categorized the fault modes of bedding rock slopes into three distinct modes, namely, integral slip mode, collapse fault mode, and slip tensile fracture mode. Zhang Zhuoyuan et al. (2009) [14] summarized the evolution of the fault modes of rock slopes as follows: sliding fault along weak structural planes, collapse, and destruction. Zhu Hanya et al. (2004) [15–17] compared the fault of bedding rock slopes with the buckling instability of slabs and beams. They provided a criterion to determine stability displacement. Thanks to years of extensive research and analysis, the procedure used to analyze and study slope stability has matured. The methodology and work flow of our study can be described as follows: recognition and characterization of the actual slope; development of mechanical and mathematical models; application of a calculation method; and elaboration of the concluding remarks. Our slope stability research is focused on the construction of an appropriate mechanical and mathematical model, as well as on the use of reasonable calculation methods for slopes [18–24].

The stability of rock slopes is often determined by locking sections along potential sliding surfaces, which have a high bearing capacity in order to resist instability. Hongran Chen et al. (2018) [25] discovered that the physical model of a multi-locking-section slope is solely dependent on the displacement of the first locking section's volume expansion point and on the number of sections. Hongnan Qin et al. (2020) [26] proposed that the time series curve of fault deformation in the multi-locking-section slope differs significantly from the typical three-stage fault deformation theory of slopes with creep characteristics. Qifeng Guo et al. (2020) [18] considered the slope as a system and used the energy method of system stability to calculate the safety factor of rock slopes with locking segments. They also considered the weakening effect of joints and the locking effect of rock bridges.

With the rapid development of society, various types of large-scale engineering projects have been constructed. During and after their construction, it is essential to involve a great degree of slope engineering, including engineering many bedding-layer rock slopes. Especially in areas with complex geological conditions, construction inevitably involves manual excavation, which poses extremely high risks. At this point, the feasibility, safety, and economy of the entire process need to be judged by analyzing the stability of the bedding-layer rock slope. To some extent, it can also be said that the stability of the slope determines the success or failure of the project and will greatly affect the investment and benefits of the project.

Currently, research on bedding rock slope primarily focuses on stability and post-landslide treatment measures. However, there is a lack of scientific and rigorous research focused on the formation mechanism of slope instability, as well as on its prevention and on issuing timely warnings when it occurs. In this work, an experimental series is performed through the application of different loads to a bedding rock slope model in order to study the changes in its macro-characteristics and analyze its fault mechanism. These findings provide a significant reference for slope treatment and similar slope engineering.

2. Model Overview

2.1. Design of the Slope Model

The design of the slope model is shown Figure 1:

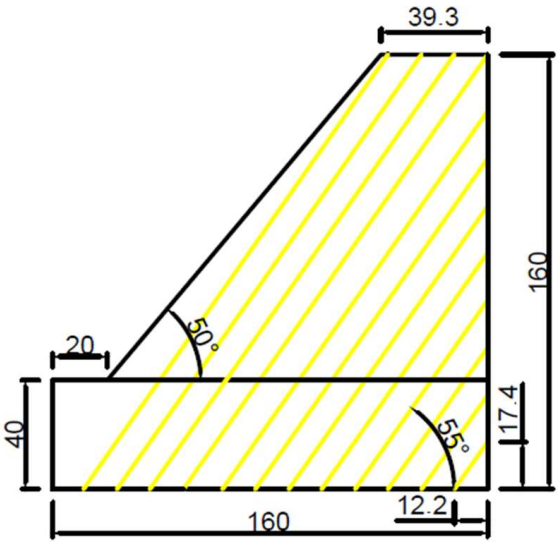

Figure 1. Design of the slope model.

2.2. Similitude Design

To guarantee precision in our experiments, it is crucial that the prototype maintains the similarity of the analogue model slope [27]. Based on the loading capacity of the test apparatus, as well as the technical parameters and other conditions, we have determined that the model length, density, and modulus of elasticity will serve as the fundamental quantities, with their respective similarity constants being represented by S_L = 64, S_ρ = 1, and S_E = 64. Table 1 contains the main similarity constants of the model slope for each physical quantity, determined based on theory.

Table 1. Main similarity constants of model slope.

Physical Quantity	Simulation Relation	Similitude Parameter
Length	S_L	64
Density	S_ρ	1.0
Elasticity modulus	$S_E = S_L S_\rho$	64
Strain	$S_\varepsilon = 1$	1.0
Internal friction angle	$S_f = 1$	1.0
Cohesion	$S_c = S_L S_\rho$	64

2.3. Slope Modeling

Based on previous conclusions [28–31], we selected barite powder, quartz sand, iron powder, gypsum, rosin, and alcohol to be the main analogue materials for this test. The mechanical test resulted in a ratio of 586.656:279.36:65.184:60:8.8:50. The physical and mechanical parameters of the test materials are presented in Table 2.

Table 2. Physical and mechanical parameters of test materials.

Density (g/cm^3)	Compressive Strength (MPa)	Tensile Strength (MPa)	Elastic Modulus (MPa)	Poisson Ratio	Internal Friction Angle (°)	Cohesion (kPa)
2.51	1.076	0.094	138.735	0.14	36.23	0.396

2.4. Distribution of Monitoring Points

This study employed displacement sensors and acoustic emission sensors to detect the sliding displacement of the slope sliding surface. The displacement sensors, numbered DH1–DH5, were used in conjunction with seven acoustic emission probes, numbered S1–S7, which were distributed uniformly on the landslide sliding surface (Figure 2).

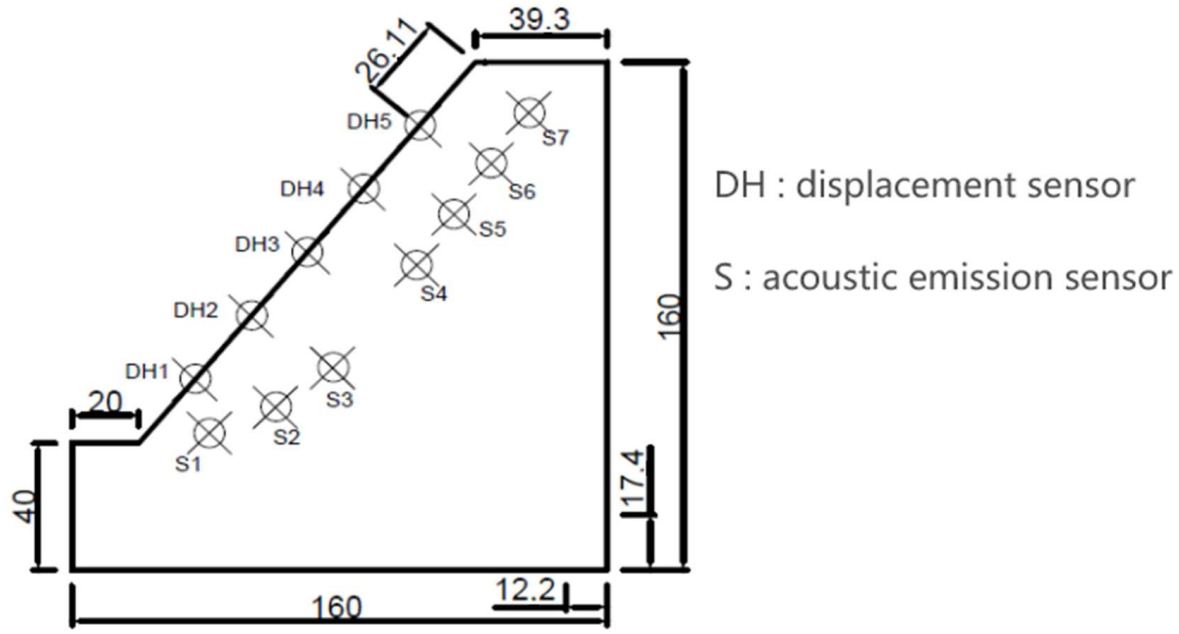

Figure 2. Distribution of measurement points.

2.5. Loading Procedure

The model was subjected to vertical loads of varying strengths until it reached the bearing critical point, after which the model collapsed. The landslide load ranged from 0.143 MPa to 1.786 MPa, divided into 22 loading grades, as shown in Table 3.

Table 3. Test loading scheme.

Test Number	Landslide Load (MPa)	Slope Loading (10^6 N)
1	0.143	0.024
2	0.286	0.048
3	0.429	0.072
4	0.500	0.084
5	0.571	0.096
6	0.643	0.108
7	0.714	0.120
8	0.786	0.132
9	0.857	0.144
10	0.929	0.156
11	1.000	0.168
12	1.071	0.180
13	1.143	0.192
14	1.214	0.204
15	1.286	0.216
16	1.357	0.228
17	1.429	0.240
18	1.500	0.252
19	1.571	0.264
20	1.643	0.276
21	1.714	0.288
22	1.786	0.300

3. Process of Slope Load Deformation Fault

DH3821 displacement sensors were fixed on the sliding surface of the slope model, and acoustic emission probes were fixed onto the side of the slope, allowing them to be connected to the corresponding acquisition system (Figure 3). The model was subjected to loads according to a predetermined loading scheme until the end of the test (Table 3), with the load being applied successively through the console of the YDM-D-type geotechnical structure model testing machine.

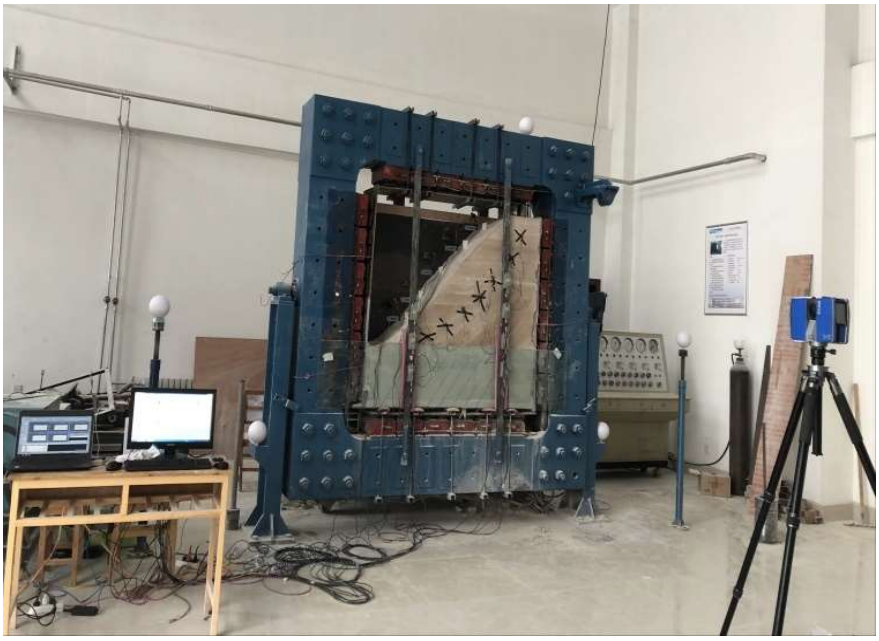

Figure 3. Test data collection process.

The DH3821 data acquisition system was used to collect the displacement response data of the model under each load condition, in conjunction with the displacement sensor and the acoustic emission acquisition system. Figure 3 illustrates the data acquisition process.

The main technical indicators of DH3821 are shown in Table 4:

Table 4. Main technical indicators of the equipment.

Main Technical Indicators		Main Technical Indicators	
Model block size	160 × 160 × 40 cm	Holding time	>48 h
Maximum load concentration	5 MPa	Maximum piston stroke of the loader	50 mm
Load concentration deviation	<5%	Area of the lower chamber of a single piston	50.27 cm^2
Uniform range of strain field	130 × 130 cm	Single piston upper chamber area	30.64 cm^2
Relative deviation of uniformity	<5%	Maximum loading oil pressure	18 MPa
Maximum chamber size	30 × 34 cm		

To observe the test process, the deformation and fault characteristics of the slope model were analyzed using a 3D laser scanner. Based on the analysis of displacement and acoustic emission data collected during the test, the slope model revealed varying degrees of fault in response to different loads [32–36].

The load was applied along successive increments ranging from 0.143 MPa to 1.786 MPa. Real-time displacement data were collected using the DH3821 data acquisition system at a frequency of 0.5 s, as Tables 5–7, Figures 4–15 below.

As Figures 4–15, the red markings on the graph represent the external manifestations of deformation and failure in the slope model. During the loading test, cracks became visible at the front and back of the model. As the load increased, cracks developed on the

middle side, right side, and slope foot, and they continued to grow as the load increased. The cracks inside the slope model eventually extended from top to bottom and connected with those at the foot of the slope. As a result, the slide surface of the slope slid significantly, forming a through-slip surface, causing complete destabilization and damage to the model.

Table 5. DH1 displacement changes.

Test Number	Landslide Load (MPa)	Displacement Change (mm)
0	0	0
1	0.143	0.03
2	0.286	0.07
3	0.429	0.09
4	0.500	0.09
5	0.571	0.11
6	0.643	0.12
7	0.714	0.14
8	0.786	0.15
9	0.857	0.18
10	0.929	0.22
11	1.000	4.8
12	1.071	4.88

Table 6. DH3 displacement changes.

Test Number	Landslide Load (MPa)	Displacement Change (mm)
0	0	0
1	0.143	0.34
2	0.286	0.89
3	0.429	1.11
4	0.500	1.71
5	0.571	2.11
6	0.643	2.51
7	0.714	2.73
8	0.786	2.86
9	0.857	3.18
10	0.929	4.85
11	1.000	5.07
12	1.071	5.28

Table 7. DH5 displacement changes.

Test Number	Landslide Load (MPa)	Displacement Change (mm)
0	0	0
1	0.143	0.66
2	0.286	0.93
3	0.429	1.07
4	0.500	3.1
5	0.571	3.55
6	0.643	3.96
7	0.714	4.54
8	0.786	5.1
9	0.857	7.09
10	0.929	8.82
11	1.000	9.59
12	1.071	9.96

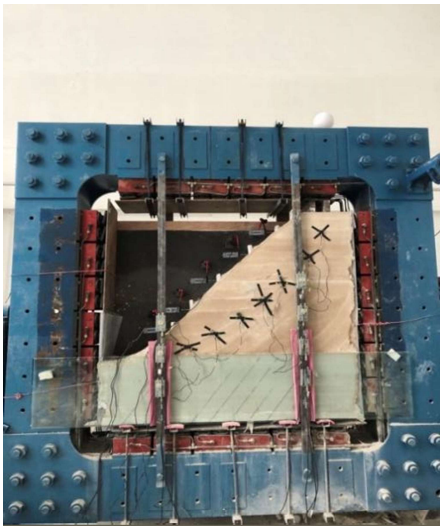

Figure 4. The landslide load is 0.143 MPa.

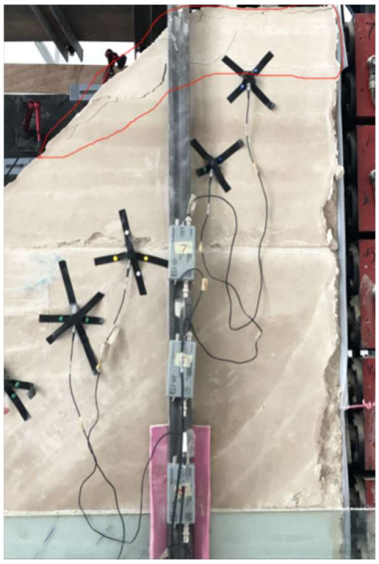

Figure 5. The landslide load is 286 Mpa.



Figure 6. The landslide load is 0.429 MPa.

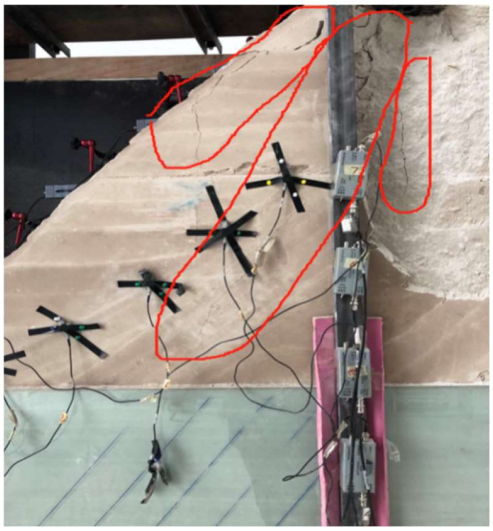

Figure 7. The landslide load is 0.500 Mpa.

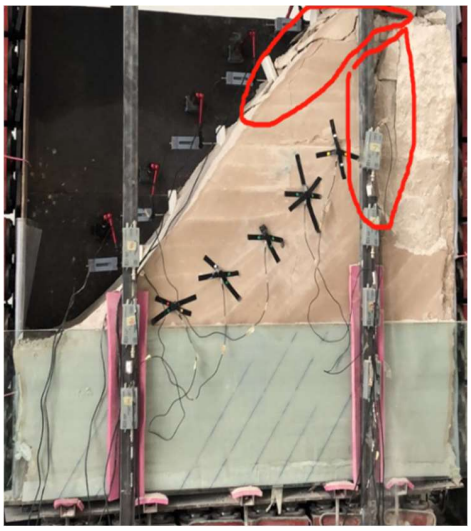

Figure 8. The landslide load is 0.571 MPa.

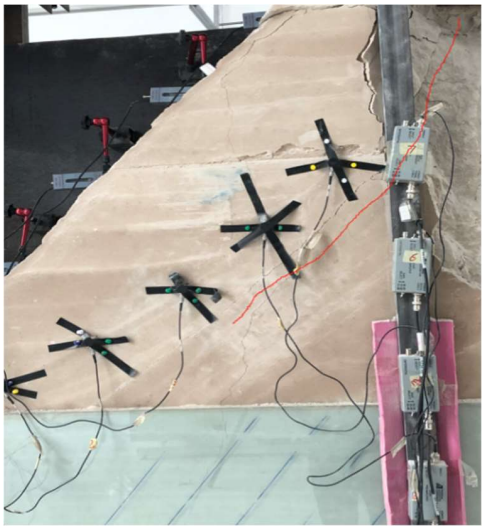

Figure 9. The landslide load is 0.643 Mpa.

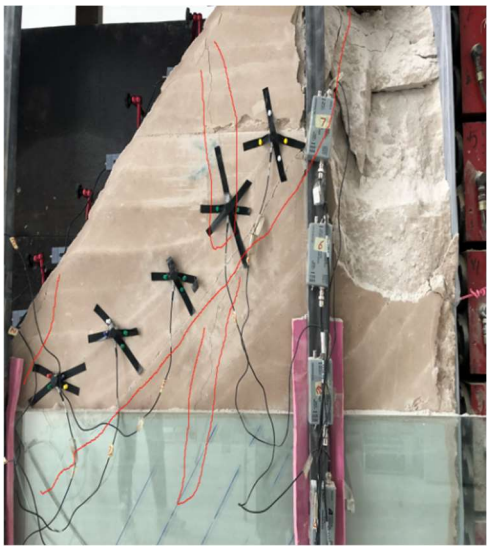

Figure 10. The landslide load is 0.714 MPa.

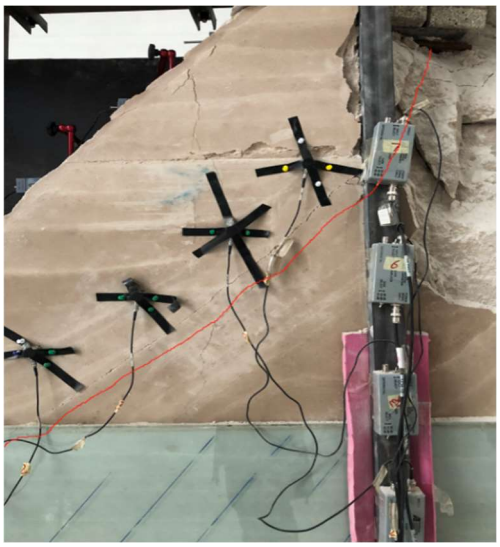

Figure 11. The landslide load is 0.786 Mpa.

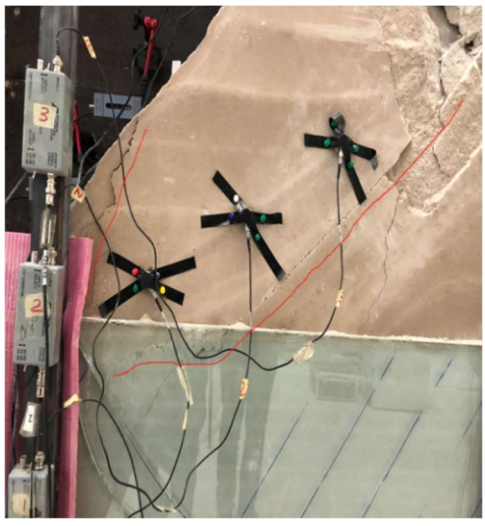

Figure 12. The landslide load is 0.857 MPa.

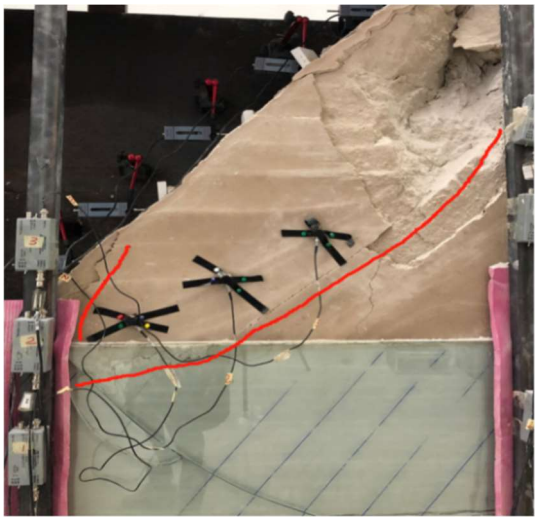

Figure 13. The landslide load is 0.929 Mpa.

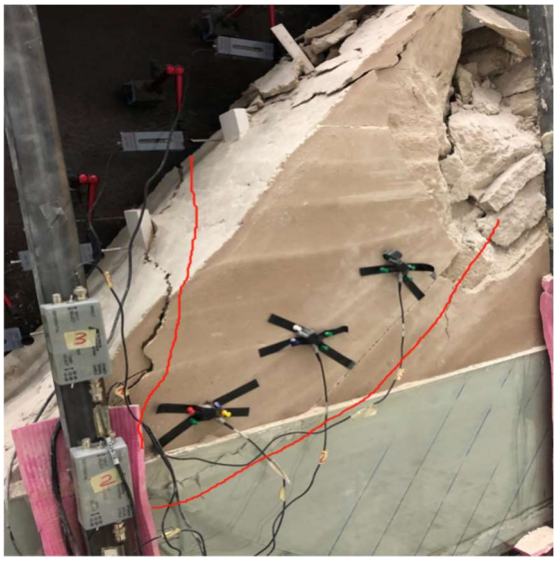

Figure 14. The landslide load is 1.000 MPa.



Figure 15. The landslide load is 1.071 MPa.

4. Data Analysis

The DH3821 data acquisition system collects real-time displacement data at a frequency of 0.5 s. Figure 16 displays the horizontal displacement of various parts of the slope for different loading intensities.

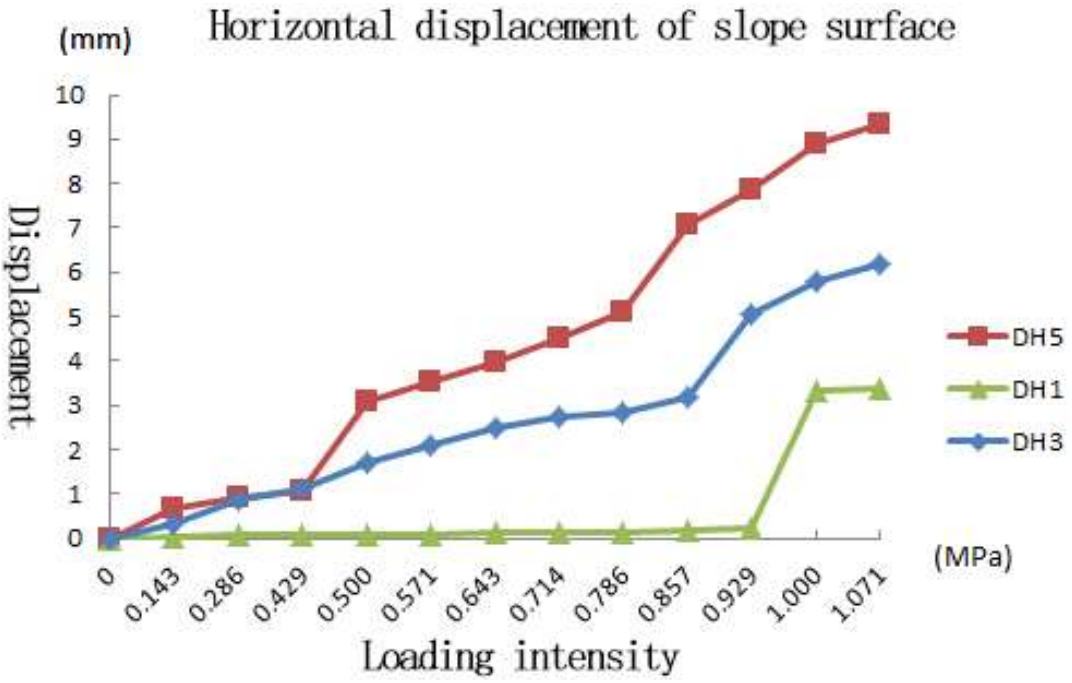

Figure 16. Change in horizontal displacement of slope.

Figure 16 displays displacement sensors DH1, DH3, and DH5 located at the bottom, middle, and top of the slope sliding surface, respectively. The curve illustrates that an increase in the strength of the vertical load on the top of the model results in an increase in the lateral displacement on the side slope.

During the initial loading stage, shear deformation primarily occurred at the top and middle sections of the slope, while the foot of the slope experienced minimal to no deformation. Under increased load, the slope experienced a sudden small change in shear deformation due to its low shear strength. This deformation gradually increased. In the middle of the slope, deformation increased steadily, but it remained smaller than that of the upper part. At the foot of the slope, deformation was minimal or nonexistent.

When the load strength increased beyond a certain point, the slope's sliding surface experienced significant shear deformation due to the absence of retaining on the free surface. Figure 4 shows that as the load strength increased step by step, DH5 at the top of the slope underwent large-scale shear deformation and fault at a load strength of 0.786 MPa, followed by DH3 in the middle of the slope at 0.857 MPa. Finally, DH1, located at the locking section of the slope foot, experienced abrupt lateral displacement at a load strength of 0.929 MPa. As the load increased, the displacement at the sliding surface of the slope decreased until the slope completely destabilized.

Figures 17 and 18 show the analysis of signal strength and energy at S1–S7 during the test based on real-time photography and video recording, which was performed using a 3D laser scanner. The analysis is based on the increase in load and the passage of time during the test.

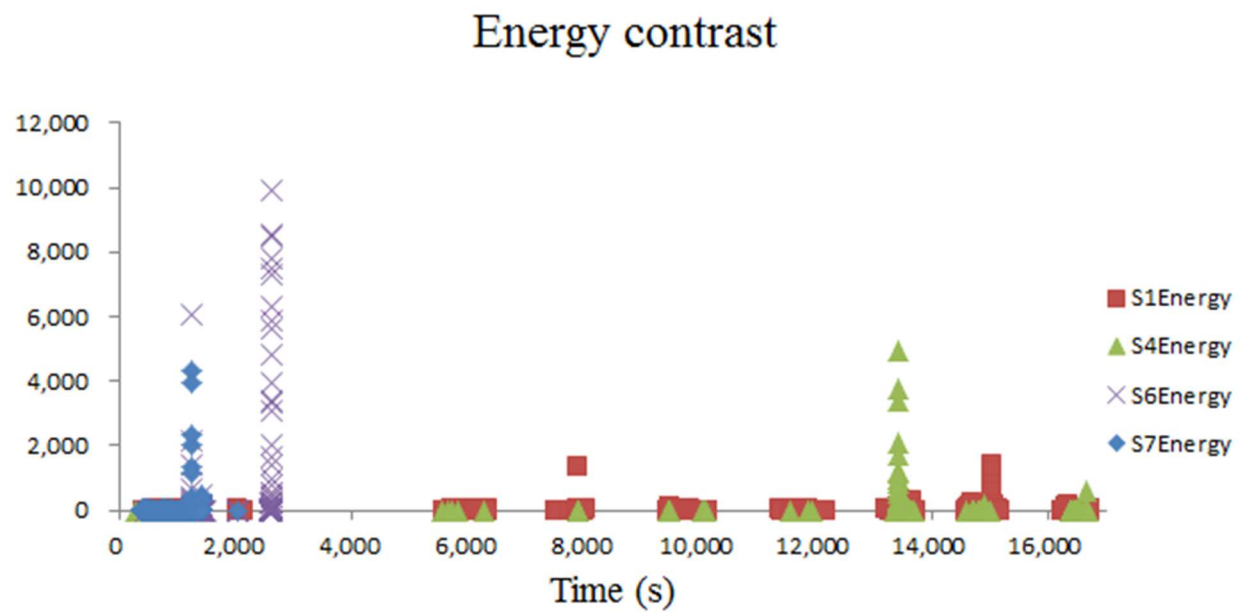

Figure 17. Signal intensity comparison on slope.

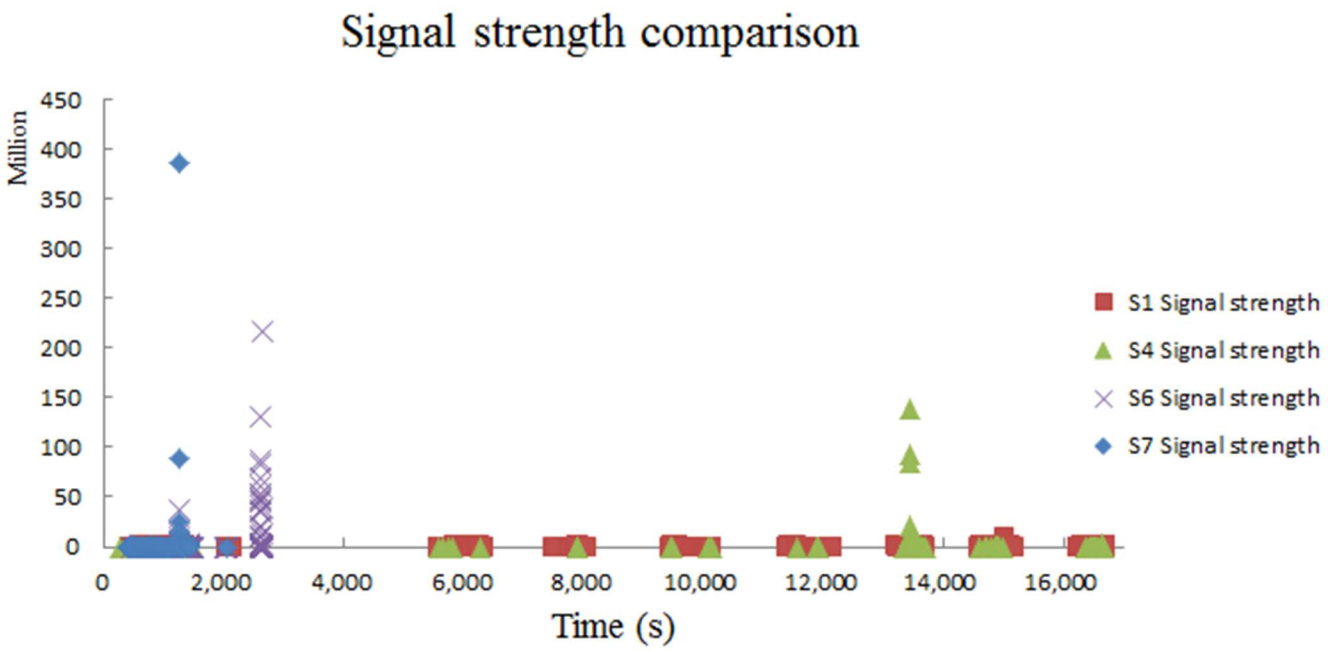

Figure 18. Energy comparison on slope.

Figures 17 and 18 demonstrate that the slope exhibited varying signal strength and energy as time and vertical load increased at its peak and near the top at around 1300 s, specifically at measurement points S7 and S6. No significant changes were observed in other areas. At around 13,500 s, the maximum peak occurred at the S4 measuring point in the middle of the slope. Finally, the maximum value was observed at the S1 measuring point located at the bottom of the slope at around 15,000 s. It can be inferred that, as the load strength increased, the displacement changed from the top of the slope to the bottom.

It is evident that the shear strength was smaller near the top of the slope sliding surface, stronger in the middle, and largest at the bottom.

5. Identification Criterion of Instability State of Locked-Type Slope

This study examines the identification criterion for the fault disaster evolution state of the inclined locking rock slope under load by observing its deformation and fault phenomenon at different levels of load strength, referring to previous research results. The rock mass loosened and deformed at the top and back of the slope model under the action of different levels of loads. During the test, a tension crack formed from the top to the bottom of the slope, and another formed at the foot of the slope. Eventually, the crack in the slope merged with the tension crack at the foot of the slope, resulting in the fault of the slope model. The deformation and fault of the slope model is here analyzed in detail, where we reveal the three stages which occurred in the evolution of slope deformation, as follows:

(1) Initial stage of deformation and faulting in the model, characterized by the stretching and opening of the rock mass at the top and back of the slope: as the load strength increases, the deformation and fault area of the slope expands, resulting in thin and downward tension cracks.
(2) Stage of development, expansion, and interlayer dislocation of slope fractures: as the load strength gradually increases, tension cracks appear in the slope, causing lateral displacement. The slope contains numerous tension cracks that may expand and extend from the top to the foot of the slope. This can cause an increase in interlayer displacement and lead to delamination and fragmentation of the model surface.
(3) Fault stage, with the formation of through cracks and large-scale slope instability: as the load strength increases, cracks within the slope expand, resulting in a strong interlayer dislocation. This causes a sharp increase in the displacement of the DH1 measuring point and a rapid rise in signal strength and energy of the S1 measuring point, defining a complete through plane from the top to the foot of the slope model, at the locking section of the slope foot. This triggers the instability and faulting of the slope model.

6. Numerical Simulation Analysis Based on FLAC 3D

6.1. Introduction to FLAC 3D

In the 1980s, British scholars Peter Cundall and Itasca developed finite difference software and applied it to the design and construction of large-scale projects such as water conservancy and civil engineering, where the software played an important role. Now, FLAC has been widely used around the world.

Based on the finite difference Joseph-Louis Lagrange algorithm, FLAC 3D can simulate the whole process of deformation and failure of the model, which can provide effective guidance for engineering design and research. Because FLAC 3D uses a hybrid discretization method that is more advanced than progressive iteration, it is more suitable for simulating problems in large deformation or torsion mechanics of rock masses; problems in simulating slope stability can be solved without obstacles. At the same time, FLAC 3D is solved by display without memory matrix, which can be used to solve large strain problems in a short time.

6.2. Numerical Model Setting

Compared to the model test, numerical simulation calculations are less restricted by particular conditions. In this paper, we used numerical simulation to analyze the fault mode of the model under different conditions and to simulate the macroscopic deformation, fault geometry, and degree of slope for different loads.

The first step in the FLAC 3D simulation calculation is the selection of the calculation model, which generalizes the actual slope model based on the research purpose and the size and complexity of the calculation model [37]. For this test, the simulation analysis uses the numerical calculation model shown in Figure 19, in which only the upper part and the sliding surface can be freely deformed, while all other surfaces are static.

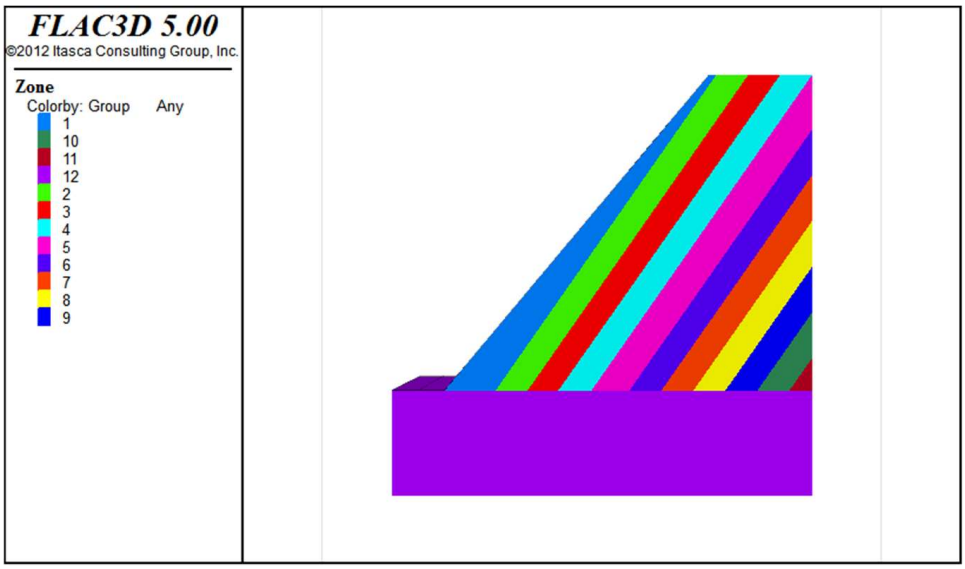

Figure 19. Numerical calculation model of the test plan.

The laboratory test set the slope model in place for more than 15 days after the completion of the backfill in order to maintain the slope model and, simultaneously, carry out the stress compensation and deformation adjustment of the slope model in advance. Therefore, the initial deformation of the model is not considered, and displacement equilibrium is performed after calculating the initial stress. This paper uses the total stress analysis method for numerical simulation.

6.3. Model Material Parameters

The setting of parameters has a direct impact on the results of numerical simulations. To ensure that the conclusions are well constrained and of a certain reference value, it is essential that we select the calculation parameters reasonably. The parameters used in this work are derived from the laboratory model tests, and the specific parameters are shown in Table 8.

Table 8. Material parameters of the numerical calculation model.

Density (g/cm^3)	Compressive Strength (MPa)	Tensile Strength (MPa)	Elastic Modulus (MPa)	Poisson Ratio	Internal Friction Angle (°)	Cohesion (kPa)
2.51	1.076	0.094	138.735	0.14	36.23	0.396

6.4. Numerical Model Results

6.4.1. Geometry of Fault Plane

The geometry of the fault plane can be obtained through the calculation and analysis of the numerical model of a bedding-locked rock slope under load. The model shows that when the slope model is in the final unstable state, it is affected by a complete continuous fault plane, resulting in the instability of the slope and the locking section. Its geometry represents a combination of a straight line and a circular arc. The shape of the sliding surface when the numerical model of the slope finally fails is shown in Figure 20.

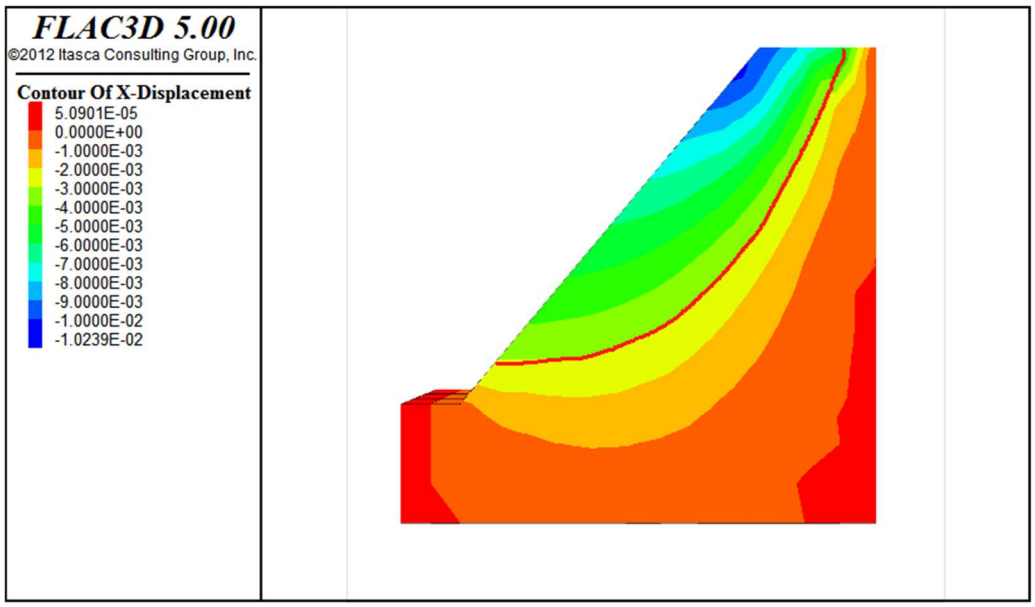

Figure 20. Numerical simulation of the shape of the sliding surface during slope instability and fault.

6.4.2. Displacement Characterization Studies

In this study, the numerical simulation slope model was calculated, and the law of the variation in its horizontal displacement with the curve of the load applied to the top of the model was analyzed (Figure 21).

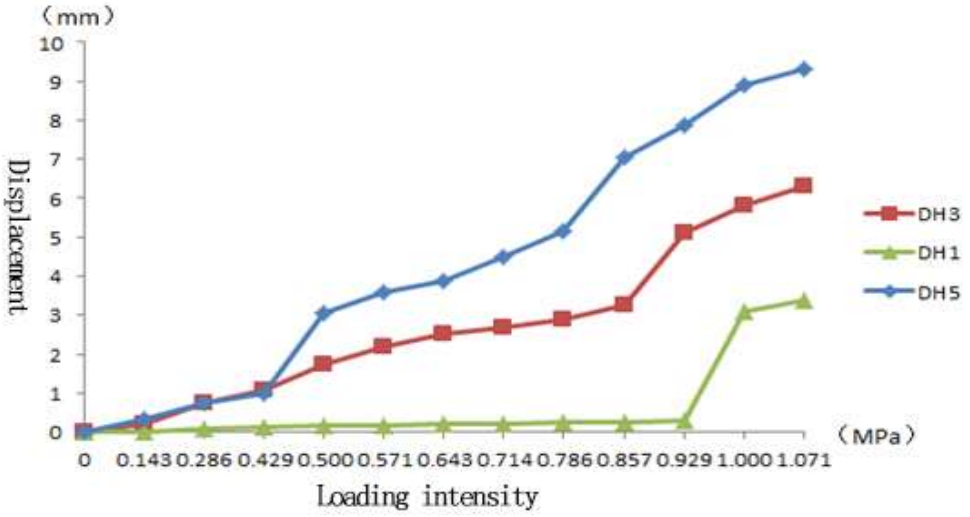

Figure 21. Horizontal displacement—top load curve.

The figure illustrates that the displacement of each measuring point increased gradually along with the load on the top surface of the side slope. Additionally, the lateral displacement was larger closer to the top surface, with a pattern of DH5 > DH3 > DH1. Between 0.929 and 1.000 MPa, DH1's displacement point mutated, resulting in a complete through crack, which caused slope instability. Maximum instability displacement was obtained at 3.37 mm. The law can also be derived from the horizontal displacement cloud map in cases where the slope numerical model is unstable. Figure 22 displays a horizontal displacement cloud image when the model is unstable.

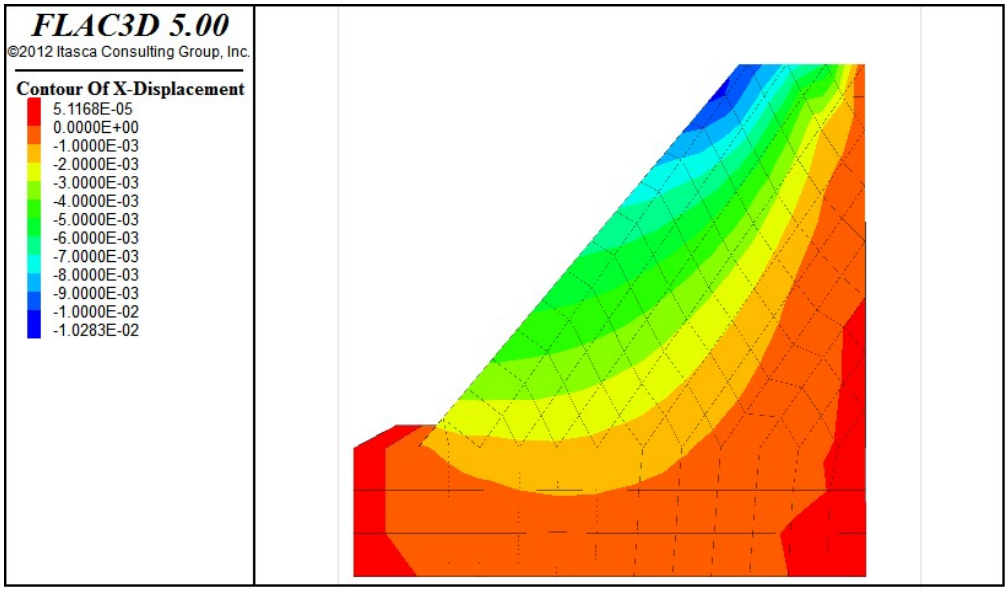

Figure 22. Horizontal displacement cloud diagram when the model is unstable.

7. Conclusions

(1) Under the influence of vertical load at the top of the slope, the rocky slope with down-layer locking exhibits local instability, primarily focused on the slope surface. The upper part of the slope features a linear slip surface, while the lower part features a circular arc slip surface, resulting in "linear + circular arc" damage geometry and a relatively flat shear surface.

(2) For vertical loading at the top of the slope, the displacements at the measurement points on the sliding surface increase proportionally along with loading. Maximum and minimum lateral displacement occurs around the top and the foot of the slope, respectively, leaving the intermediate values at the middle. In other words, the slope experiences maximum deformation near the top. Therefore, special attention should be paid to potential sliding areas during the construction and management of this type of project.

(3) Under vertical loading at the top of the slope, abrupt changes in the displacement of each measuring point on the sliding surface indicate that there was less shear strength than shear stress, resulting in slope deformation, collapse, and the occurrence of the sliding surface. The load strength required for the sudden change in displacement of the measurement points is highest at the foot of the slope, followed by the middle, and lowest at the top. The results indicate that the shear strength is greater at the locking section, with the highest value found at the foot of the slope, followed by the middle and the top.

(4) The evolution of slope deformation can be divided into three stages: the loose deformation stage at the slope top and back; the stage of crack development, extension, and interlayer misalignment; and the stage of complete through crack formation and complete instability damage of the slope. Thus, the process of the deformation and damage of a rocky slope under loading conditions can be described as follows: load-induced loosening and deformation at the top and back of the slope and crack development, expansion, and interlayer misalignment, as well as tension crack expansion, at the foot of the slope. The latter can expand and intensify interlayer misalignment, leading to the destruction of the locking section and ultimately causing the destabilization of the entire slope. Therefore, it is important that the monitoring procedures of the locking section are focused on the bottom of the slope to effectively predict slope stability.

8. Prospect

Due to limitations in experimental conditions, the loading method used in this experiment is relatively single. In this experimental study, only the application of loads at the top of the slope was considered, without considering the possible effects of applying loads in other directions or dynamic loads on it. Future research and learning may consider applying lateral or dynamic loads to study the displacement response law and deformation failure law of slopes under their action.

Author Contributions: X.H. completed the experiment, processed the data, and wrote the article. J.D. conducted the experiment, processed the data, and revised the article. X.Y. conducted the conception of the experiment, processed the data, and revised the article. H.G. helped complete the experiment and revised the article. All authors have read and agreed to the published version of the manuscript.

Funding: This study was financially supported by the National Natural Science Foundation of China (grant no. 41825018) and the National Key Research and Development Project of China (Grant No. 2019YFC1509704).

Institutional Review Board Statement: Not applicable.

Informed Consent Statement: Not applicable.

Data Availability Statement: The data underlying this article will be shared on reasonable request to the corresponding author.

Conflicts of Interest: The authors declare that there are no conflicts of interest regarding the publication of this paper.

References

1. Lv, Z. Slope Stability Analysis Based on Deformation Analysis Theory. Master's Thesis, Central South University, Changsha, China, 2010.
2. Teng, W.; Yun, X.; Sun, S. Application of Finite element strength Reduction Method to Study the Relationship between slope rate and stability. *Highw. Automob. Transp.* **2013**, 119–122.
3. Hu, L.; Li, X.; Wen, S. The Stability Research of Slope and Its Developing Trend. *Min. Res. Dev.* **2000**, 7–8+27.
4. Li, S. Research on Three-Dimensional Intelligent Information System for Slope Safety Assessment. Master's Thesis, Graduate School of Chinese Academy of Sciences (Wuhan Institute of Rock and Soil Mechanics), Wuhan, China, 2005.
5. Chen, G. Stability Analysis of Layered Rock Slope. Master's Thesis, Chongqing University, Chongqing, China, 2008.
6. Qiang, S. Study on Monitoring and Prediction Method of the Stability of Layered Rock Slope in Mountainous expressway. Master's Thesis, Graduate School of Chinese Academy of Sciences, Wuhan Institute of Rock and Soil Mechanics, Wuhan, China, 2007.
7. Tao, G. Study on the Stability of Rocky Slopes with Smooth Layers. Master's Thesis, Xi'an University of Technology, Xi'an, China, 2009.
8. Yang, G.; Ye, H.; Wu, F.; Qi, S.; Dong, J. Dynamic response characteristics and failure mechanism of anti-dip stratified rock slope by shaking table model test. *Chin. J. Rock Mech. Eng.* **2012**, *31*, 2214–2221.
9. Feng, X.; Jiang, Q.; Zhang, H. Shaking Table Test on Seismic Response of Rock Slope. *J. Vib. Meas. Diagn.* **2018**, *38*, 575–582.
10. Huang, R.; Guo, L.I.; Nengpan, J. Shaking Table Test on Strong Earthquake Response of Stratified Rock Sslopes. *Chin. J. Rock Mech. Eng.* **2013**, *32*, 865–875.
11. Hui, Q.; Xiaotao, Y.; Hua, T.; Xu, C.; Hao, Y. Method of Stress Field and Stability Analysis of Bedding Rock Slope Considering Excavation Unloading. *KSCE J. Civ. Eng.* **2023**, *27*, 4205–4214.
12. Chen, Z.; Hu, X.; Bu, X. Effect of weak intercalation on failure mode of rock slopes under seismic excitation. *Nat. Hazards* **2020**, *105*, 1–19. [CrossRef]
13. Zhang, J. Sensitivity Analysis on the Stability of Bedding Rock Slope and Its Influencing Factors. Master's Thesis, Shaoxing University of Arts and Sciences, Shaoxing, China, 2021.
14. Zhang, Z.; Wang, S.; Wang, L.; Huang, R.; Xu, Q.; Tao, L. *Principles of Engineering Geological Analysis*; Geological Publishing House: Beijing, China, 2009.
15. Zhu, H.; Ma, M.; Shang, Y. Analysis of buckling failure of consequent rock slope. *J. Zhejiang Univ. Eng. Sci.* **2004**, *38*, 1144–1149.
16. Liu, J. Development of Geogical Engineering Monitoring Information on System. *J. Eng. Geol.* **1997**, *5*, 335–356.
17. Li, Y.; Yang, Z.; Wang, Z. Displacement Theory of Structure Stability For Rock Mass Bbedding Slope. *Chin. J. Rock Mech. Eng.* **2000**, *19*, 747–750.
18. Guo, Q.; Pan, J.; Cai, M.; Zhang, Y. Analysis of Progressive Failure Mechanism of Rock Slope with Locked Section Based on Energy Theory. *Energies* **2020**, *13*, 1128. [CrossRef]

19. Chi, M. Study on the Characteristics and Formation Mechanism of Landslide on the Contact Surface of Accumulation and Bedrock. Master's Thesis, Chang'an University, Chang'an, China, 2016.
20. Tang, Z. Analysis of Slope Stability and Reinforcement in Bailong Stadium. Master's Thesis, Kunming University of Science and Technology, Kunming, China, 2006.
21. Yang, S. Study on Slope Instability Failure Mode in East Jianshan Phosphate Mine. Master's Thesis, Kunming University of Science and Technology, Kunming, China, 2011.
22. Leng, J. Application Research on the Instability and Reinforcement of Bedding Rock Slope. Master's Thesis, Scientific Research Institute of Ministry of Railways, Beijing, China, 2005.
23. Li, J. A Systematic Study of Landslides on the South and North Slopes of Guanshan Mountain in Foping County, Shaanxi Province. Master's Thesis, Chang'an University, Chang'an, China, 2008.
24. Sun, Y.; Yao, B.; Xu, B. Review and prospect of mine slope stability research. *J. Eng. Geol.* **1998**, 18–24+74.
25. Chen, H.; Qin, S.; Xue, L.; Yang, B.; Zhang, K. A physical model predicting instability of rock slopes with locked segments along a potential slip surface. *Eng. Geol.* **2018**, *242*, 34–43. [CrossRef]
26. Qin, H.; Ma, H.; Yu, Z. Research on the deformation and failure mode of rock slope with multiple locking segment failure characteristics. *IOP Conf. Ser. Earth Environ. Sci.* **2020**, *570*, 062002.
27. Han, X. Deformation and Failure Model Test of Bedding Layer Rock Slope. Master's Thesis, North China University of Water Resources and Electric Power, Zhengzhou, China, 2020.
28. Zhang, Q.; Liu, D.; Jia, C.; Shen, X.; Liu, J.; Duan, K. Development of geomechanical model similitude material for salt rock oil-gas storage medium. *Rock Soil Mech.* **2009**, *30*, 3581–3586.
29. Wang, H.; Li, S.; Zhang, Q.; Guo, X. Development of a new geomechanical similar material. *Chin. J. Rock Mech. Eng.* **2006**, *25*, 1842–1847.
30. Dong, J.; Yang, J.; Yang, G.; Wu, F.; Liu, H. Research on similar proportioning test of model test based on orthogonal design. *J. China Coal Soc.* **2012**, *37*, 44–49.
31. Dong, J.; Liu, Z.; Yang, J.; Li, G. Application of Uniform Design in Similar Material Proportioning Test of Physical Model Test. *J. North China Inst. Water Resour. Hydropower* **2013**, *34*, 39–41.
32. Dong, J.Y.; Yang, J.H.; Wu, F.Q.; Yang, G.X.; Huang, Z.Q. Large-scale shaking table test research on acceleration response rules of bedding layered rock slope and its blocking mechanism of river. *Chin. J. Rock Mech. Eng.* **2013**, *32*, 3861–3867.
33. Yang, G.; Wu, F.; Dong, J.; Qi, S. Study on dynamic response and deformation failure mechanism of rock slope under earthquake. *Chin. J. Rock Mech. Eng.* **2012**, *31*, 696–702.
34. Dong, J.Y.; Yang, G.X.; Wu, F.Q.; Qi, S.W. The large-scale shaking table test study of dynamic response and failure mode of bedding rock slope under earthquake. *Rock Soil Mech.* **2011**, *32*, 2977–2983.
35. Liu, H.; Geng, Z.; Wang, Z.; Niu, L.; Xu, F. Research on dynamic response of anti-dip rock slope and influence of ground motion parameters. *J. North China Univ. Water Resour. Electr. Power (Nat. Sci. Ed.)* **2019**, *40*, 70–76. (In Chinese)
36. Li, K.; Shang, Y.; He, W.; Jiang, Y. Characteristics and Mechanism of Bedding Rock Slope Failure:A Case Study on No.5 Slope at Wutai-Yuxian Expressway. In *Academic Paper Collection of Institute of Geology and Geophysics, Chinese Academy of Sciences—Engineering Geology and Water Resources Research*, 15th ed.; Atlantis Press: Amsterdam, The Netherlands, 2015.
37. Wang, M.; Liu, K.; Yang, G.; Xie, J. Three-dimensional slope stability analysis using laser scanning and numerical simulation. *Geomat. Nat. Hazards Risk* **2017**, *8*, 997–1011. [CrossRef]

Disclaimer/Publisher's Note: The statements, opinions and data contained in all publications are solely those of the individual author(s) and contributor(s) and not of MDPI and/or the editor(s). MDPI and/or the editor(s) disclaim responsibility for any injury to people or property resulting from any ideas, methods, instructions or products referred to in the content.